A&A 530, A83 (2011)
DOI: 10.1051/0004-6361/201116597

Astronomy & Astrophysics

A chemical inventory of the S-type AGB star χ Cygni based on *Herschel*/HIFI observations of circumstellar line emission⋆

The importance of non-LTE chemical processes in a dynamical region

F. L. Schöier[1,⋆⋆], M. Maercker[2], K. Justtanont[1], H. Olofsson[1], J. H. Black[1], L. Decin[3,4], A. de Koter[4,5], and R. Waters[4,6]

[1] Onsala Space Observatory, Dept. of Earth and Space Sciences, Chalmers University of Technology, 43992 Onsala, Sweden
e-mail: hans.olofsson@chalmers.se
[2] University of Bonn, Argelander-Institut für Astronomie, Auf dem Hügel 71, 53121 Bonn, German
[3] Instituut voor Sterrenkunde, Katholieke Universiteit Leuven, Celestijnenlaan 200D, 3001 Leuven, Belgium
[4] Sterrenkundig Instituut Anton Pannekoek, University of Amsterdam, Science Park 904, 1098 Amsterdam, The Netherlands
[5] Astronomical Institute, Utrecht University, Princetonplein 5, 3584 CC Utrecht, The Netherlands
[6] SRON Netherlands Institute for Space Research, Sorbonnelaan 2, 3584 CA Utrecht, The Netherlands

Received 27 January 2011 / Accepted 31 March 2011

ABSTRACT

Context. S-type AGB stars (C/O ≈ 1) are thought to be transition objects from M-type (O-rich) AGB stars to carbon stars and as such are interesting objects in themselves. Of particular interest is to determine accurate circumstellar properties and molecular abundances, due to their predicted sensitivity to the photospheric C/O-ratio.
Aims. Presented here are new sensitive sub-millimetre line observations of molecules towards the S-type AGB star χ Cyg, using the HIFI instrument on-board the *Herschel* Space Observatory. The observed lines predominantly probe warm gas relatively close to the central star.
Methods. Detailed, non-LTE, radiative transfer modelling has been used in order to interpret the circumstellar molecular line observations performed using HIFI, assuming a spherically symmetric, smooth, accelerating wind.
Results. Lines from common molecules such as H_2O, CO and SiO, which are expected to be abundant in an S-type AGB star, are clearly detected (as well as some of their isotopologues) in the HIFI spectra. In addition, we detect lines from carbon-bearing molecules such as HCN and CN. The CO line modelling indicates that the mass-loss rate has not undergone any significant modulations during the past ≈1000 yr. The derived o-H_2O fractional abundance is $\approx 7 \times 10^{-6}$, i.e., lower than those obtained for a small sample of M-type AGB stars but higher than what has been derived for a few carbon stars. We further obtain a p-H_2O fractional abundance of $\approx 5 \times 10^{-6}$ giving an o/p-ratio of ≈1.4. Molecular line cooling is dominated by H_2O only in a region close to the star ($\lesssim 6 \times 10^{14}$ cm). The SiO abundance is estimated to be $\approx 1 \times 10^{-5}$. The $^{12}CO/^{13}CO$ ratio is 43 ± 6. The high-excitation rotational lines clearly probe the acceleration region of the stellar wind ($\lesssim 2 \times 10^{15}$ cm) and put constraints on dynamical wind models. We are unable to fit consistently the combined ground-based and HIFI data for HCN and CN.
Conclusions. The derived H_2O abundance is reasonably consistent with recent chemical model predictions and so is the SiO abundance. The o/p-ratio of ≈1.4 supports a chemical formation under non-LTE conditions for the H_2O molecules, and the presence of carbon-bearing molecules at relatively large abundances is also indicative of the importance of non-LTE chemical processes in regulating the circumstellar chemistry. The velocity field derived from the molecular line modelling is consistent with that obtained from solving for the wind dynamics through the coupled momentum equations of the dust and gas particles.

Key words. circumstellar matter – stars: AGB and post-AGB – radio lines: stars – stars: mass-loss

1. Introduction

AGB stars of spectral type S have C/O ratios close to unity (within ≈5%), and an excess of s-process elements in their atmospheres. These objects have for some time now been considered as possible transition objects from M-type (O-rich) AGB stars (C/O < 1) to carbon (C-rich) stars (C/O > 1), and are as such particularly interesting to study from a chemical point of view. However, there is a lack of observational data (in part due to their low relative number compared to the two other chemical types) in particular in the form of circumstellar line observations of molecules other than CO. Recently, Ramstedt et al. (2006, 2009) determined the circumstellar properties of a large sample of 40 S-type AGB stars using multi-transitional CO and SiO mm-line observations. When comparing to studies of similar samples of M-type and carbon stars, the results show clearly that the mass-loss rate does not depend on the chemistry of the star. In contrast, the wind kinematics is different for the three chemistries; the C-rich CSEs have, on average, higher expansion velocities, and there is a high fraction of very low wind velocities among the S-type and M-type objects. It was also shown that the mass-loss rate and wind velocity dependence is as expected for a dust-driven wind.

⋆ *Herschel* is an ESA space observatory with science instruments provided by European-led Principal Investigator consortia and with important participation from NASA.
⋆⋆ Passed away 14 January 2011.

Table 1. Summary of observations.

Setting	Tuning frequency [GHz]	η_{mb}	Polarization	Frequency [GHz]	Molecule	Transition	I_{mb} [K km s^{-1}]	E_{up} [K]
1	1868.55 (USB)	0.65	H	1867.749 (USB)	o−H_2O	$5_{3,2}-5_{2,3}$	1.92	732
16	1842.04 (USB)	0.66	H	1841.346 (USB)	CO	16−15	14.0	752
4	1717.57 (USB)	0.66	H	1716.770 (USB)	o−H_2O	$3_{0,3}-2_{1,2}$	18.6	197
6	1163.75 (USB)	0.69	H + V	1162.912 (USB)	o−H_2O	$3_{2,1}-3_{1,2}$	1.59	305
				1153.127 (LSB)	o−H_2O	$3_{1,2}-2_{2,1}$	7.23	249
				1151.985 (LSB)	CO	10−9	14.0	304
				1151.452 (LSB)	HCN	13−12	1.49	387
7	1112.98 (USB)	0.70	H + V	1113.343 (USB)	p−H_2O	$1_{1,1}-0_{0,0}$	7.87	53
				1112.832 (USB)	^{29}SiO	26−25	0.70	502
				1101.350 (LSB)	^{13}CO	10−9	1.36	291
				1099.711 (LSB)	^{30}SiO	26−25	0.38:	496
8	1096.70 (LSB)	0.70	H + V	1097.365 (LSB)	o−H_2O	$3_{1,2}-3_{0,3}$	4.19	249
9	1001.70 (USB)	0.70	H + V	991.329 (LSB)	^{13}CO	9−8	1.23	238
				987.927 (LSB)	p−H_2O	$2_{0,2}-1_{1,1}$	7.69	101
10	969.76 (LSB)	0.70	H + V	970.315 (LSB)	p−H_2O	$5_{2,4}-4_{3,1}$	0.67	599
11	764.94 (USB)	0.71	H + V	752.033 (LSB)	p−H_2O	$2_{1,1}-2_{0,2}$	3.61	137
17	692.47 (USB)	0.71	H + V	694.293 (USB)	SiO	16−15	2.58	197
				691.473 (USB)	CO	6−5	14.3	116
				690.552 (USB)	H^{13}CN	8−7	0.34:	149
				680.264 (LSB)	CN	$6_{6.5}-5_{5.5}$	2.74	114
				680.047 (LSB)	CN	$6_{5.5}-5_{4.5}$	3.56	114
12	659.60 (USB)	0.71	H + V	661.067 (USB)	^{13}CO	6−5	1.49	111
13	620.90 (USB)	0.71	H + V	620.304 (USB)	HCN	7−6	4.45	119
				607.599 (LSB)	SiO	14−13	2.60	219
14	559.78 (LSB)	0.71	H + V	560.326 (LSB)	SiO	$v=1$, 13−12	0.20	1360
				557.179 (LSB)	^{29}SiO	13−12	0.76	187
				556.936 (LSB)	o−H_2O	$1_{1,0}-1_{0,1}$	2.91	61

A combined modelling of CO rotational lines in the far-infrared (from $J = 14 \rightarrow 13$ up to $J = 37 \rightarrow 36$ observed using the ISO satellite) and in the mm and sub-mm bands (from $J = 1 \rightarrow 0$ up to $J = 4 \rightarrow 3$ observed using ground-based instruments) of extreme carbon stars was performed by Ryde et al. (1999) and Schöier et al. (2002). The various excitation conditions of the observed lines allow the circumstellar envelope (CSE) characteristics to be probed over a large radial range. The results indicate that the studied stars have not gone through any major modulation of their mass-loss rates during the past $\sim 10^4$ yr. A limiting factor of the lines observed by ISO is that they were not spectrally resolved. Recently, more or less periodic mass-loss-modulations have been detected in a few number of extreme carbon stars using observations of interstellar light scattered in the CSE (Mauron & Huggins 1999, 2000, 2006). However, the favoured interpretation is not a mechanism intrinsic to the star but one that involves a binary companion that periodically modulates a more or less constant mass-loss rate from the AGB star (Huggins et al. 2009). Again, the interpretation is limited due to a lack of direct kinematical information.

In the detailed modelling of circumstellar H_2O line emission for a number of M-type AGB stars, observed using the ISO and Odin satellites, the derived ortho-H_2O abundances are $\sim 10^{-4}$ (Justtanont et al. 2005; Maercker et al. 2008, 2009). The recent analysis of *Herschel* data of the M-type AGB star IK Tau confirms this (Decin et al. 2010c). Such H_2O abundances can be explained by a stellar atmosphere equilibrium chemistry. In contrast, to explain the detection of H_2O in the extreme carbon star IRC +10216 (Melnick et al. 2001; Hasegawa et al. 2006), even higher abundances in the carbon star V Cyg (Neufeld et al. 2010), and the ubiquitous occurrence of H_2O in CSEs around carbon stars (Neufeld et al. 2011), requires some effective non-equilibrium chemical process (Willacy 2004), the influx of H_2O through the evaporation of icy-bodies (Melnick et al. 2001), or, as recently suggested by Decin et al. (2010a), the penetration of interstellar ultraviolet photons deep into a clumpy CSE, thereby affecting the chemistry. A study of the S-type AGB star χ Cyg suggests that this type of stars has an intermidiate circumstellar H_2O abundance (Justtanont et al. 2010).

Presented here is a spectral scan of circumstellar molecular line emission towards the S-type AGB star χ Cyg. The spectrally resolved molecular line observations were performed using the HIFI instrument on-board the *Herschel* Space Observatory. They have been supplemented by a careful and detailed numerical excitation analysis in order to determine the physical and chemical structure of the CSE. This set of data extends the sub-set presented in Justtanont et al. (2010).

2. Observations

2.1. HIFI observations

χ Cyg was observed in March and April 2010 using the HIFI heterodyne receiver (de Graauw et al. 2010) on board the *Herschel* Space Observatory (Pilbratt et al. 2010) as part of HIFISTARS, a guaranteed time key project. Some of the observations were already published in Justtanont et al. (2010) but are also included here for completeness. The final spectra, as recorded by the WBS backend and binned to a velocity resolution of 3 km s^{-1}, are presented in Fig. 1. The observed lines are summarized in Table 1. The setting refers to the numbering within the HIFISTARS project (which is retained here for ease of identification of

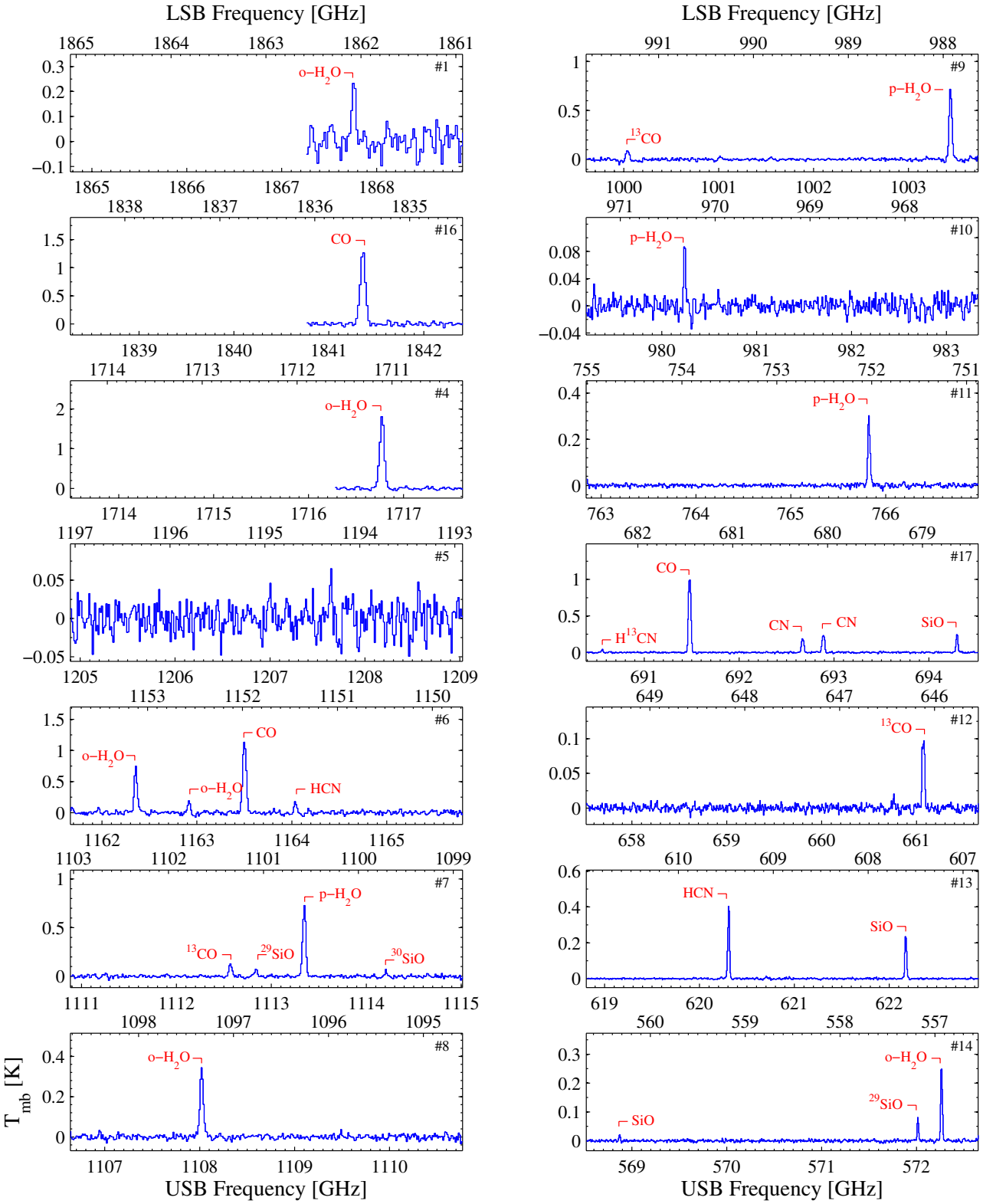

Fig. 1. Observed spectra of χ Cyg using the HIFI instrument presented at a velocity resolution of 3 km s^{-1}. Spectral lines above the 3σ level are indicated by their molecular name (for transition information see Table 1). The spectral setting within HIFISTARS is indicated in the upper right corner of each spectrum.

the detected lines). In total we detect 30 spectral lines corresponding to 6 different molecular species (and a number of their isotopomers). Spectra in the same setting but at orthogonal polarizations (H and V) were averaged when possible, to improve the signal-to-noise ratio. In the high frequency settings (1, 4, and 16) only a part of the H-polarization spectrum could be used due to ripples, or a high noise level, in the remaining part of the spectrum as well as in the V-polarization spectrum. The absolute calibration uncertainty of the intensity scale is estimated to be (HIFI ICC, priv. com.) ±16% for HIFI bands

1, 2 and 5 (480−800 GHz and 1120−1250 GHz) and ±32% for bands 3, 4, 6 and 7 (800−1120 GHz and 1410−1910 GHz). In the case of a weak detection, marked with a (:) in Table 1, we adopt an uncertainty of ±50%.

The spectra are dominated by strong rotational emission lines from common molecules like CO, H_2O and SiO, as expected for an S-type AGB star. Relatively strong line emission from carbon-based molecules such as HCN and CN is also present. Also, rotational lines within the first vibrationally excited state ($v = 1$) of SiO are detected. The observed spectral lines are mainly of thermal origin, with excitation energies of ∼50−1000 K (see Table 1), and effectively probe a large part of the CSE, in particular the warm inner regions.

2.2. Complementary observations

In order to probe also the external cooler part of the circumstellar molecular envelope, low excitation transitions (∼5−100 K), from ground based single-dish (e.g., the OSO 20 m, IRAM 30 m, and 15 m JCMT telescopes) and interferometric observations (from Plateau de Bure) are included in the analysis. Combined with the HIFI observations essentially the full radial range of the CSE can be probed and, if present, modulations in the mass-loss rate and chemical gradients may be identified. The references to this complementary set of molecular line data are given in Table A.1, except for the PdBI CO data that are taken from Castro-Carrizo et al. (2010) and the PdBI SiO data from Lucas et al. (1992). The calibration of the intensity scale for these data have an uncertainty of ≈±20%

In addition, the data used to produce the SED constraining the dust radiative transfer modelling are reported in Table B.1.

3. Radiative transfer analysis

χ Cyg is an S-type Mira variable with a period of 408 days (Kholopov et al. 1999). The revised Hipparcos distance (Knapp et al. 2003) of 150 pc is adopted throughout the paper.

The CSE is assumed to be spherically symmetric, and smooth, with an isotropic, radially increasing velocity field (keeping the mass-loss rate constant). For the molecular line excitation analysis well-tested, non-LTE and non-local, spectral line radiative transfer codes (based on the Monte Carlo and ALI methods), as presented in Schöier & Olofsson (2001), Justtanont et al. (2005) and Maercker et al. (2008, 2009) are used. The codes have also been benchmarked to high accuracy against other non-LTE radiative line transfer codes (van Zadelhoff et al. 2002; Maercker et al. 2008). The dust continuum radiative transfer analysis is performed using the well-tested and publicly available dust radiative transfer code Dusty (Ivezićs & Elitzur 1997).

The best-fit models were determined from a chi-square statistic defined as

$$\chi^2 = \sum_{i=1}^{N} \frac{[I_{\mathrm{mod},i} - I_{\mathrm{obs},i})]^2}{\sigma_i^2}, \quad (1)$$

where I is the total velocity-integrated line intensity (or flux density in the case of SED modelling), σ_i is the uncertainty in observation i, and the summation is done over all independent observations N. This gives the total χ^2 from which the reduced χ^2 (which is a measure of the quality of the fit) can be calculated using $\chi^2_{\mathrm{red}} = \chi^2_{\mathrm{tot}}/(N - p)$, where p is the number of adjustable parameters in the fitting prodedure.

Table 2. Derived stellar and circumstellar parameters.

Parameter	Dust/Dyn	CO
$L_\star$	$8000\,L_\odot$	···
$T_\star$	2600 K	···
τ_{10} [a]	0.05	···
r_{i}	2.0×10^{14} cm	···
$\upsilon(\infty)$	···	$8.5\,\mathrm{km\,s^{-1}}$
$\dot{M}$	$4.8 \times 10^{-7}\,M_\odot\,\mathrm{yr^{-1}}$	$7.0 \times 10^{-7}\,M_\odot\,\mathrm{yr^{-1}}$
Ψ [b]	2.7×10^{-3}	1.2×10^{-3}
α	0.95	0.5−1.5

Notes. [(a)] Dust optical depth at 10 μm. [(b)] The dust-to-gas mass-loss-rate ratio.

3.1. Dust radiative transfer and dynamical modelling

We start by modelling the observed SED using the dust continuum radiative transfer code Dusty (Ivezićs & Elitzur 1997). The input parameters are the adopted Hipparcos distance and dust grain parameters. The dust grains are assumed to consist of amorphous silicate (Justtanont & Tielens 1992). For simplicity, the dust grains are further assumed to be spherical and of the same size with a radius $a_{\mathrm{gr}} = 0.05\,\mu$m and a mass density $\rho_{\mathrm{gr}} = 3\,\mathrm{g\,cm^{-3}}$. The adjustable parameters are the dust condensation temperature (T_{c}; from which the dust condensation radius, r_{c}, can be calculated), the stellar black-body temperature ($T_\star$), and the optical depth (τ_λ; here taken at 10 μm) through the dusty envelope which sets the absolute dust density scale. In addition, the dust temperature structure is calculated self-consistently. The modelling procedure is described in more detail in Schöier et al. (2002) and Ramstedt et al. (2008). For χ Cyg the dust condensation temperature is only constrained to ≤1300 K and we adopt a characteristic value of 900 K where the dust condensation is assumed to be essentially complete. The corresponding radius (r_{c}) is adopted as the inner radius (r_{i}) in the modelling that follows.

The dust radiative transfer modelling is in turn coupled with a dynamical model (solving the coupled momentum equations of the dust and gas particles) as described in Ramstedt et al. (2008) but with a few major updates. Most significantly, Dusty models now use the density structure of an expanding wind obtained from the dynamical model and the dynamical model in turn includes the correct dust opacity structure (from Dusty) for attenuating the stellar radiation field throughout the CSE. The dust-to-gas mass-loss-rate ratio (Ψ) is modified in the dynamical modelling in order to match the terminal gas velocity (υ_∞) as determined from CO observations. The two numerical models are iterated (a few times) between one another in order to reach convergence in the derived velocity fields (dust and gas) and dust density structure. This allows for an estimate of the gas-mass-loss rate from the dynamical model ($\dot{M}_{\mathrm{dyn}}$). The derived stellar and circumstellar parameters are summarized in Table 2. We note that the circumstellar gas velocity structure of χ Cyg is well represented over the full radial range (to within a few %) by a velocity law of the form (Lamers & Cassinelli 1999)

$$\upsilon(r) = \upsilon_0 + (\upsilon(\infty) - \upsilon_0)\left(1 - \frac{r_{\mathrm{i}}}{r}\right)^{\alpha} \quad (2)$$

where $\upsilon_0 = 3.0\,\mathrm{km\,s^{-1}}$, $\alpha = 0.95$ and $\upsilon(\infty) = 8.5\,\mathrm{km\,s^{-1}}$. This is a significantly more shallow velocity law compared with that derived by Schöier et al. (2006a) for the high-mass-loss rate carbon star IRC +10216, where $\alpha = 0.2$, based on a detailed radiative transfer analysis of SiO interferometric observations in

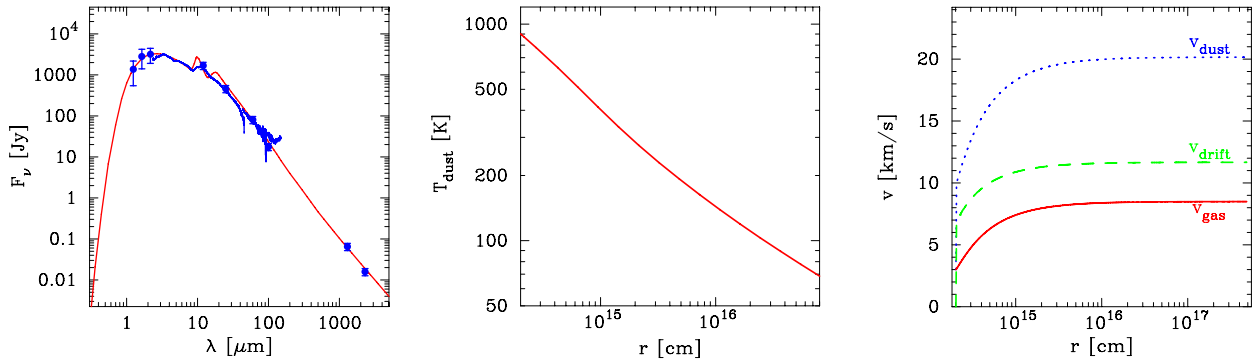

Fig. 2. *Left* – Dust radiative transfer model (red solid line) for the S-type AGB-star χ Cyg overlaid on observations (blue points). *Middle* – Derived dust temperature structure. *Right* – Wind velocities of the dust and gas, as a functions of radial distance, derived from the dynamical model.

the ground vibrational state and, in particular, SiO ro-vibrational lines in the infra-red by Keady & Ridgway (1993). In contrast, Decin et al. (2010c) derive $\alpha \approx 1-2$ from fitting HIFI line observations obtained for the M-type AGB star IK Tau, which is significantly more shallow than obtained from their dynamical model. All the results of the molecular line emission modelling below are obtained using an $\alpha = 0.95$.

The best fit model for χ Cyg is presented in Fig. 2 where the derived SED, dust temperature structure, and velocity structures are shown. The reduced χ^2-value for the best fit SED model is 2.3 using $L_\star = 8000\,L_\odot$, $T_\star = 2600$ K, $T_c = 900$ K (gives an inner radius $r_i = 2.0 \times 10^{14}$ cm; the instantaneous radius where dust formation is complete) and $\tau_{10} = 0.05$. From the dynamical modelling, a dust-to-gas ratio of $\Psi = 2.7 \times 10^{-3}$ and a gas-mass loss rate of $\dot{M} = 4.8 \times 10^{-7}\,M_\odot\,\mathrm{yr}^{-1}$ are obtained.

3.2. CO line modelling

Using the output from the combined dust radiative transfer and dynamical modelling we perform the excitation analysis of the CO multi-transitional line observations. The dust grains are distributed throughout the CSE and their absorption and thermal reemission of photons are taken explicitly into account in the molecular excitation analysis (Schöier et al. 2002). In total 10 (7 different) rotational lines are included in the analysis, with excitation energies for the upper rotational level in the range ≈5−600 K, potentially probing a large radial range of the CSE. For the velocity field we adopt the analytical fit in Eq. (2) and let α be an adjustable parameter in the modelling (in order to determine the velocity field from the observational data), together with the the gas-mass-loss rate ($\dot{M}$). The energy-balance equation is solved self-consistently including relevant heating and cooling terms. Dust-gas collisions provide the dominant heating term of the gas (e.g., Goldreich & Scoville 1976)

$$H_{\rm dg} = \frac{3}{8} m_{\rm H_2}^2 n_{\rm H_2}^2 \frac{\Psi}{a_{\rm gr}\rho_{\rm gr}} \frac{\upsilon_{\rm dr}^3(r)}{1 + \frac{\upsilon_{\rm dr}(r)}{\upsilon(r)}}, \quad (3)$$

where $m_{\rm H_2}$ and $n_{\rm H_2}$ are the mass and number density of H_2 molecules, respectively. The drift velocity, $\upsilon_{\rm dr}(r)$, is taken from the dynamical modelling. The dust-gas collisional heating is then further controlled via the h-parameter, containing a simple combination of the dust-to-gas mass-loss-rate ratio and the size and mass density of individual dust grains (Schöier & Olofsson 2001)

$$h = \left(\frac{\Psi}{1.0 \times 10^{-2}}\right)\left(\frac{0.05\,\mu\mathrm{m}}{a_{\rm gr}}\right)\left(\frac{2.0\,\mathrm{g\,cm^{-3}}}{\rho_{\rm gr}}\right). \quad (4)$$

We let the h-parameter be a third adjustable parameter that can be constrained from multi-transitional observations due to their sensitivity to the kinetic gas temperature (see, e.g., discussion in Schöier & Olofsson 2001). Molecular line cooling is dominated by that provided by H_2O and CO, which are calculated directly from the excitation analysis presented here. More details on the CO modelling can be found in Schöier & Olofsson (2001).

The ^{12}CO and ^{13}CO molecular data, used in the non-LTE excitation analysis, includes rotational transitions up to $J = 40$ in both the ground and first vibrational states. For CO the energy levels, transition frequencies and Einstein A coefficients were taken from Chandra et al. (1996). The CO-H_2 collisional rate coefficients are taken from Yang et al. (2010) and have been calculated for rotational levels going up to $J = 40$, covering collisional temperatures from 1 K up to 3000 K. The separate rate coefficients for collisions of CO with para- and ortho-H_2 have been weighted together assuming an ortho/para-H_2 ratio of 3.

Molecular line cooling (or heating under some circumstances) can be calculated once the level populations are known (typically this is done during each iteration after iteration number 5). Since the level populations contain all the information of the radiative transfer, a general expression for the cooling rate C (in erg s^{-1} cm^{-3} and defined to be positive for net cooling) is obtained from considering all possible collisional transitions (e.g., Crosas & Menten 1997; van der Tak et al. 2007)

$$C = n_{\rm H_2} \sum_l \sum_{u>l} (n_l \gamma_{lu} - n_u \gamma_{ul}) h\nu_{ul}. \quad (5)$$

As the collision rate coefficients γ_{lu} and γ_{ul} are assumed to be in detailed balance at the kinetic temperature, it is possible for net heating to occur ($C < 0$) in the CSE, for transitions where $T_{\rm ex} > T_{\rm kin}$, due to strong radiative excitation in a hot external radiation field. Molecular line cooling in the case of χ Cyg comes from CO and H_2O and is calculated directly from the level populations in the excitation analysis. As the CO and H_2O radiative transfer is performed separately a first model containing only CO line cooling is performed. The kinetic temperature structure obtained is then used in the H_2O excitation analysis and its line cooling is calculated. This is in turn included in the CO modelling as an extra cooling term. For consistency, this requires iteration of the CO and H_2O line modelling, however, convergence of the kinetic temperature in this case is fast (within two iterations).

Due to the large size of the CO molecular envelope compared to the primary beam at the PdB interferometer the brightness distributions from the models were corrected for the beam pattern. The models were then converted to the uv-plane and the same samplings as performed during the observations were applied to

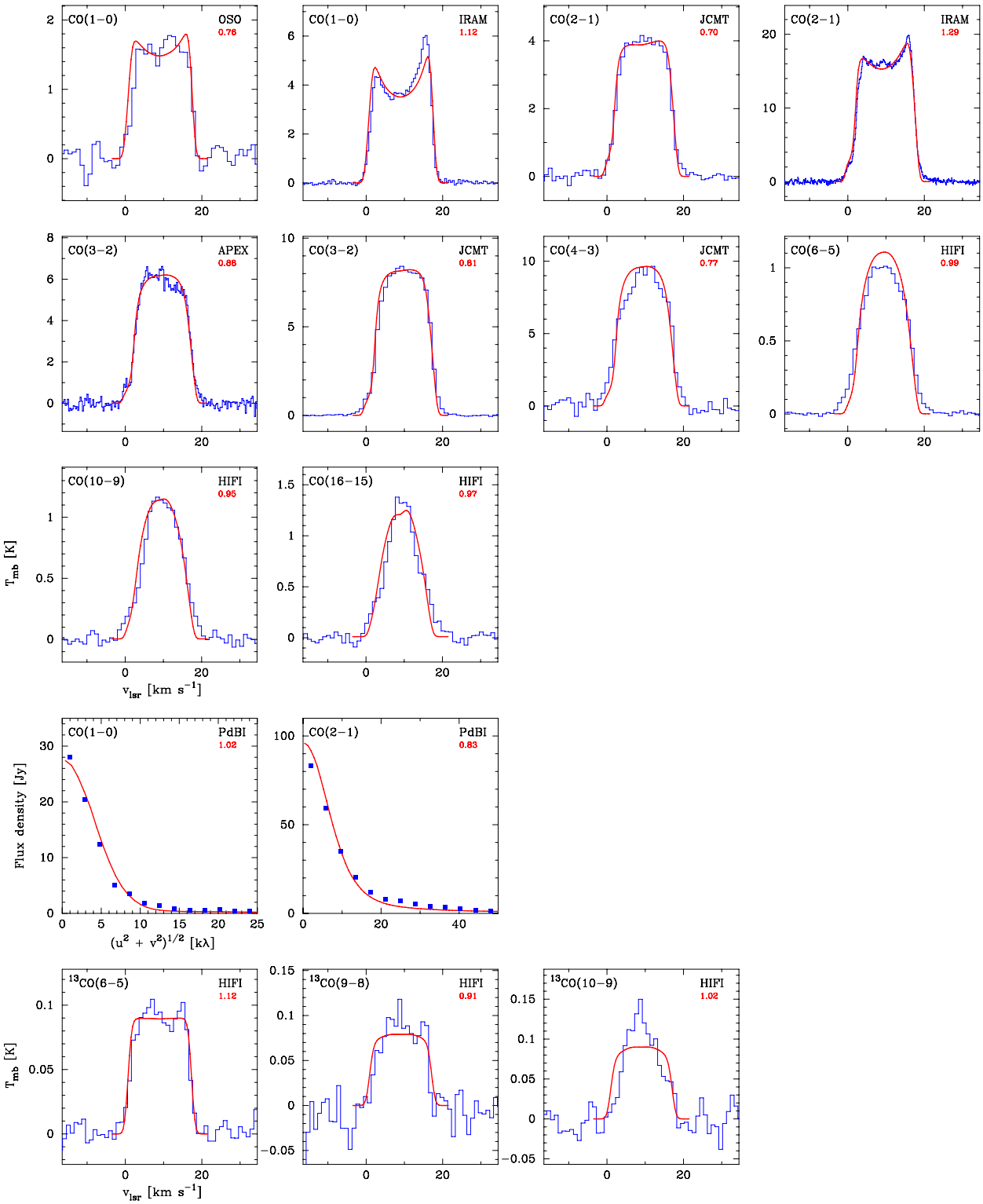

Fig. 3. CO model (solid lines) for the S-type AGB-star χ Cyg overlaid on observations (histograms and points). Models have been scaled by the indicated factor (obtained from requiring that the velocity-integrated intensities are equal to the observed ones). Also shown are derived brightness distributions (solid lines) overlaid on interferometric observations using the PdBI (blue points from Castro-Carrizo et al. 2010). A ^{12}CO/^{13}CO ratio of 43 was used.

the visibilities from the model. This procedure is described in more detail in Schöier et al. (in prep.), where a large sample of AGB stars has been mapped in CO line emission at the PdBI as part of the COSAS large survey programme (Castro-Carrizo et al. 2010).

The analysis is carried out using a χ^2-statistic (see Eq. (1)) based on the observed and modelled velocity-integrated line intensities. The best fit model has a reduced χ^2-value of 1.8 and is presented in Fig. 3, where also the fits to the PdBI data are shown. The H_2 gas mass-loss rate is derived to be $7.0 \times 10^{-7}\,M_\odot\,\mathrm{yr}^{-1}$ (adopting a CO/H_2 abundance ratio of 6×10^{-4}) with $h = 0.08$, translating into $\Psi = 1.2 \times 10^{-3}$ using the dust parameters from Sect. 3.1. The half-power radius of the CO envelope is 3.5×10^{16} cm. Using the same envelope parameters

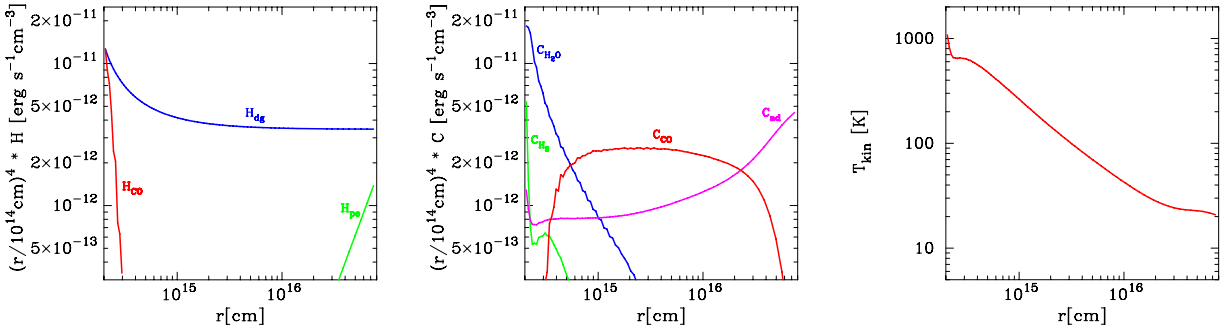

Fig. 4. Dominating heating (*left*, CO = CO lines, dg = dust gas collisions, pe = photoelectrons) and cooling (*middle*, H_2 = H_2 lines, H_2O = H_2O lines, CO = CO lines, ad = adiabatic expansion) terms in the CSE around χ Cyg, and the derived gas temperature structure (*right*).

we obtain a ^{13}CO fractional abundance of $1.4 \pm 0.2 \times 10^{-5}$ (with a reduced χ^2 value of 0.3; 3 observed transitions) . This gives a ^{12}CO/^{13}CO ratio of 43 ± 6. The best-fit ^{13}CO model is shown in Fig. 3. The derived circumstellar parameters are summarized in Table 2.

The line profiles are very well reproduced using a velocity profile following Eq. (2) with $\alpha = 0.95$, as derived from the dust modelling. However, once the best-fit model with $\alpha = 0.95$ was obtained new model results were computed for different values of α (keeping everything else the same). Although this is not a consistent procedure, it gives a feeling for the constraints on the velocity field set by the line data. It is clear that the CO line data puts limited constraints on α, roughly to the range 0.5−1.5.

The derived temperature structure and CO line cooling in the CSE around χ Cyg are presented in Fig. 4. CO line cooling ($C_{\rm CO}$) is dominating in a region of the envelope from where most of the warm emission detected by HIFI originates. We also note that in the innermost part of the wind CO lines actually heat the gas. In the cooler external regions adiabatic expansion provides the dominant cooling ($C_{\rm ad}$). This region is best probed by low-energy rotational line emission observed with ground-based telescopes. The heating is dominated by dust grain collisions throughout the CSE ($H_{\rm dg}$ in Fig. 4), while the photoelectric heating is negligible for this relatively low-mass-loss-rate CSE ($H_{\rm pe}$ in Fig. 4).

3.3. Circumstellar molecular excitation analysis

3.3.1. Fractional abundance distribution

For molecules other than CO the same modelling detail is retained. With the density and temperature structures now already derived (for the gas and dust) the remaining parameters to be determined from the various molecular lines are their fractional abundance distributions (relative to H_2). The fractional abundance distribution is assumed to be described by a Gaussian

$$f(r) = f_0 \exp\left(-\left(\frac{r}{r_{\rm e}}\right)^2\right), \quad (6)$$

as an approximation to a photodissociation-limited molecular envelope. The size of the molecular emitting region ($r_{\rm e}$) and the initial fractional circumstellar abundance (f_0) are the adjustable parameters in the modelling.

In addition, the velocity field is adjusted (α in Eq. (2)) in order to see if better constraints than provided by the CO modelling can be obtained.

3.3.2. H_2O modelling

For the radiative transfer modelling of H_2O we adopt the ALI-method (Rybicki & Hummer 1991, 1992), which is fully capable of coping with the high optical depths present in the circumstellar lines from water vapor, also for low-mass loss rate objects such as χ Cyg. Ng-acceleration has been included to further speed up convergence (Ng 1974). Our ALI-algorithm has been extensively tested and used already for modelling of H_2O data from the Odin and ISO satellites and in preparatory work for HIFI (Justtanont et al. 2005; Maercker et al. 2008, 2009).

For H_2O the energy levels, transition frequencies, and Einstein A coefficients were taken from the HITRAN database (Rothman et al. 2008), and the radiative transfer include the 45 lowest levels in each of the ground vibrational state, the first excited bending mode ($v_2 = 1$), and the asymmetric streching mode ($v_3 = 1$). The collisional rate coefficients are from Faure et al. (2007) and cover temperatures from 20 K up to 2000 K and all rotational energy levels in the ground vibrational state up to the location of the first vibrationally excited state. The separate rate coefficients for collisions of para-H_2 and H_2O and ortho-H_2 with H_2O were weighted together assuming an ortho/para-H_2 ratio of 3. In the modelling ortho-H_2O and para-H_2O are treated as separate molecular species.

The adopted extent of the H_2O molecular envelope is based on the chemical modelling of Netzer & Knapp (1987). For the circumstellar parameters of χ Cyg this value is 3.6×10^{15} cm. After fixing the envelope extent only the initial abundance (f_0) is left as an adjustable parameter. The derived ortho-H_2O abundance is $7.0 \pm 1.0 \times 10^{-6}$ (with a reduced χ^2 value of 0.8; 6 observed transitions) and a para-H_2O abundance of $5.0 \pm 1.0 \times 10^{-6}$ (with a reduced χ^2 value of 0.6; four observed transitions). The best-fit models are presented in Fig. 5. The derived circumstellar o/p-ratio is 1.4 ± 0.3. The derived H_2O line cooling in the case of χ Cyg is presented in Fig. 4. Line cooling from H_2O ($C_{\rm H_2O}$) is only dominating in a small region of the CSE very close to the central star ($\lesssim 6.0 \times 10^{14}$ cm). Finally, we note that as opposed to the case for the M-stars there is no strong o-$H_2O(5_{32}$–$4_{41})$ maser line in χ Cyg, most likely an effect of a lower H_2O abundance in an S-star.

Constraints on the velocity field are weak ($\alpha > 0$) within reasonable values of α, i.e., there is a velocity gradient also through the H_2O line emitting region. Finally we note that there is an asymmetry in most line profiles (the line shape peak is slightly shifted to the blue) that is not possible to fit using the adopted circumstellar model.

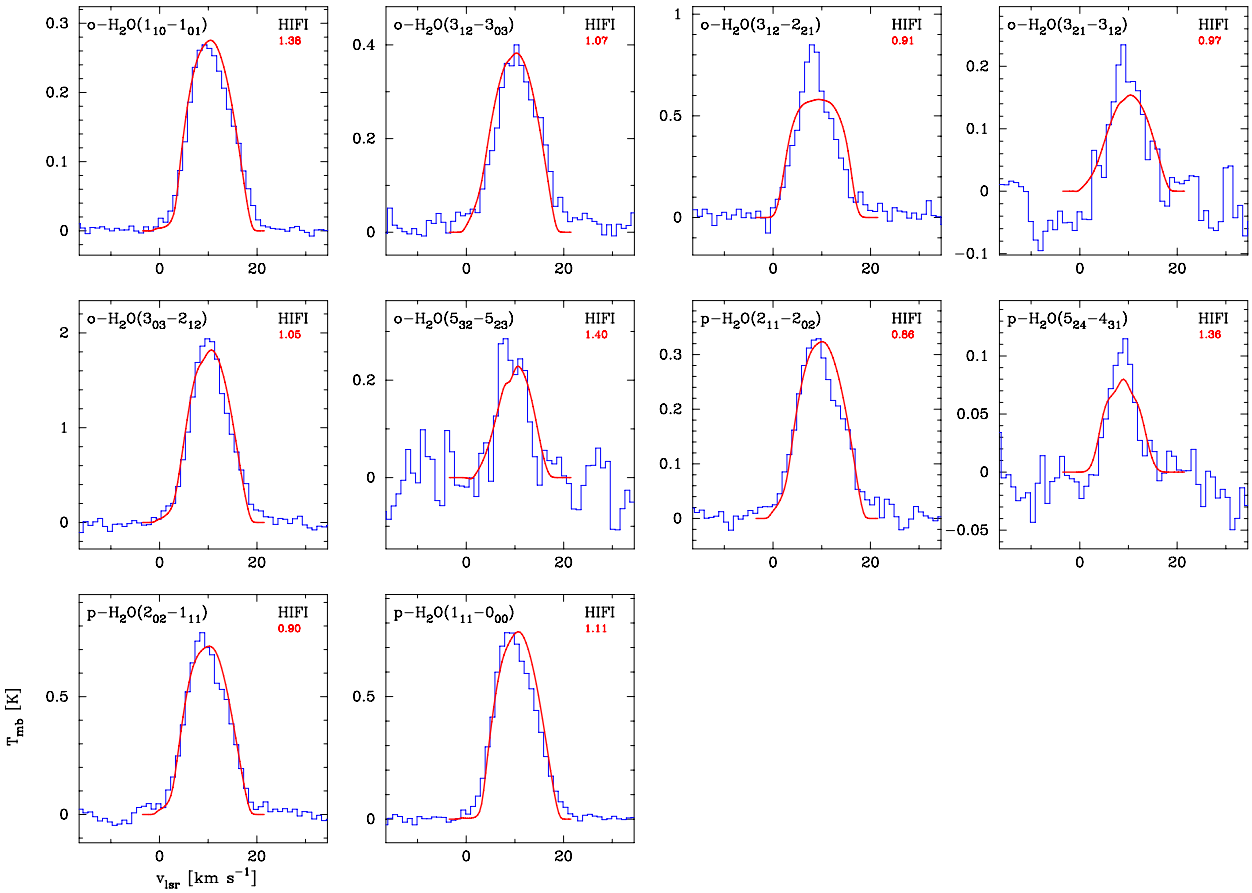

Fig. 5. H_2O model (solid lines) for the S-type AGB-star χ Cyg overlaid on observations (histograms). Models have been scaled by the indicated factor (obtained from requiring that the velocity-integrated intensities are equal to the observed ones).

3.3.3. SiO modelling

Energy levels, transition frequencies and Einstein A coefficients for SiO (for all observed isotopes) from within the first two vibrational states ($v = 0, 1$) were taken from CDMS (Müller et al. 2001, 2005). The Einstein A coefficients for the ro-vibrational transitions were calculated using the electric dipole moment measured by Raymonda et al. (1970). The collisional rates are taken from Dayou & Balança (2006) and were calculated for temperatures in the range from 10 to 300 K including energy levels up to $J = 26$ for collisions with He. This set of rate coefficients was subsequently scaled by a factor 1.38 to represent collisions with H_2, and extrapolated to include energy levels up to $J = 40$ and collisional temperatures up to 2000 K. For details on the extrapolation, see Schöier et al. (2005).

The SiO line emission from the rotational transitions in the ground vibrational state is well modelled using a single Gaussian abundance distribution with a fractional abundance of $1.3 \pm 0.2 \times 10^{-5}$. This model has a $\chi^2_{\rm red} = 1.6$ for one adjustable parameter and $N = 6$, with the other adjustable parameter (the SiO envelope size) best constrained by the PdBI data to $\approx 5.0 \times 10^{15}$ cm (Fig. 6). In this model, however, the (weak) line emission from the rotational transition in the $v = 1$ vibrational state comes out a factor of five too low, and it is not included in the analysis. The best fit model is presented in Fig. 6. For the velocity field, the SiO line spectra only constrain α to within $\approx 0.3-1.5$. There is the same tendency for an asymmetry in the line profiles as discussed above for the H_2O lines.

One possible explanation for the weakness of the $v = 1$ lines is that the abundance of SiO is higher in the warmer region closer to the star (Schöier et al. 2004; Schöier et al. 2006a,b; Decin et al. 2010b). This could be an effect due to adsorption of SiO onto dust grains in the dust forming region, that lowers the SiO fractional abundance further out in the wind. Including a dust model that takes this effect into account is beyond the scope of this paper and instead we limit ourselves to get some crude numbers on any possible chemical gradient in the fractional abundance of SiO in the inner accelerating and warm part of the CSE around χ Cyg. Adding a compact high-abundance component with a characteristic size of $r_c \approx 1.0 \times 10^{15}$ cm (where the abundance is drastically altered) significantly improves the fit to the emission lines in the $v = 1$ state, while at the same time only marginally affecting those in the $v = 0$ ground state. We find that a fractional abundance distribution that drastically decreases from 5.0×10^{-5} (at r_i) in the inner wind to 1.0×10^{-5} in the outer part best reproduces the observations. Such a model has a $\chi^2_{\rm red} = 1.2$ with two adjustable parameters and $N = 7$.

In addition, three high excitation isotopic lines are detected, two ^{29}SiO lines and one ^{30}SiO line, in the CSE around χ Cyg. The derived ^{29}SiO fractional abundance is $1.6 \pm 0.4 \times 10^{-6}$ (with a reduced χ^2 value of 0.03; 2 observed transitions) giving a ^{28}SiO /^{29}SiO abundance ratio of 8 ± 2. We obtain a ^{30}SiO fractional abundance of 7.0×10^{-7} (with an uncertainty of $\approx \pm 50\%$) that gives a ^{28}SiO /^{30}SiO abundance ratio of 19 ± 8. The best fit models are presented in Fig. 6.

3.3.4. HCN modelling

HCN is a linear molecule with three different vibrational modes: the CH stretching mode ν_1, the CN stretching mode ν_3, and the

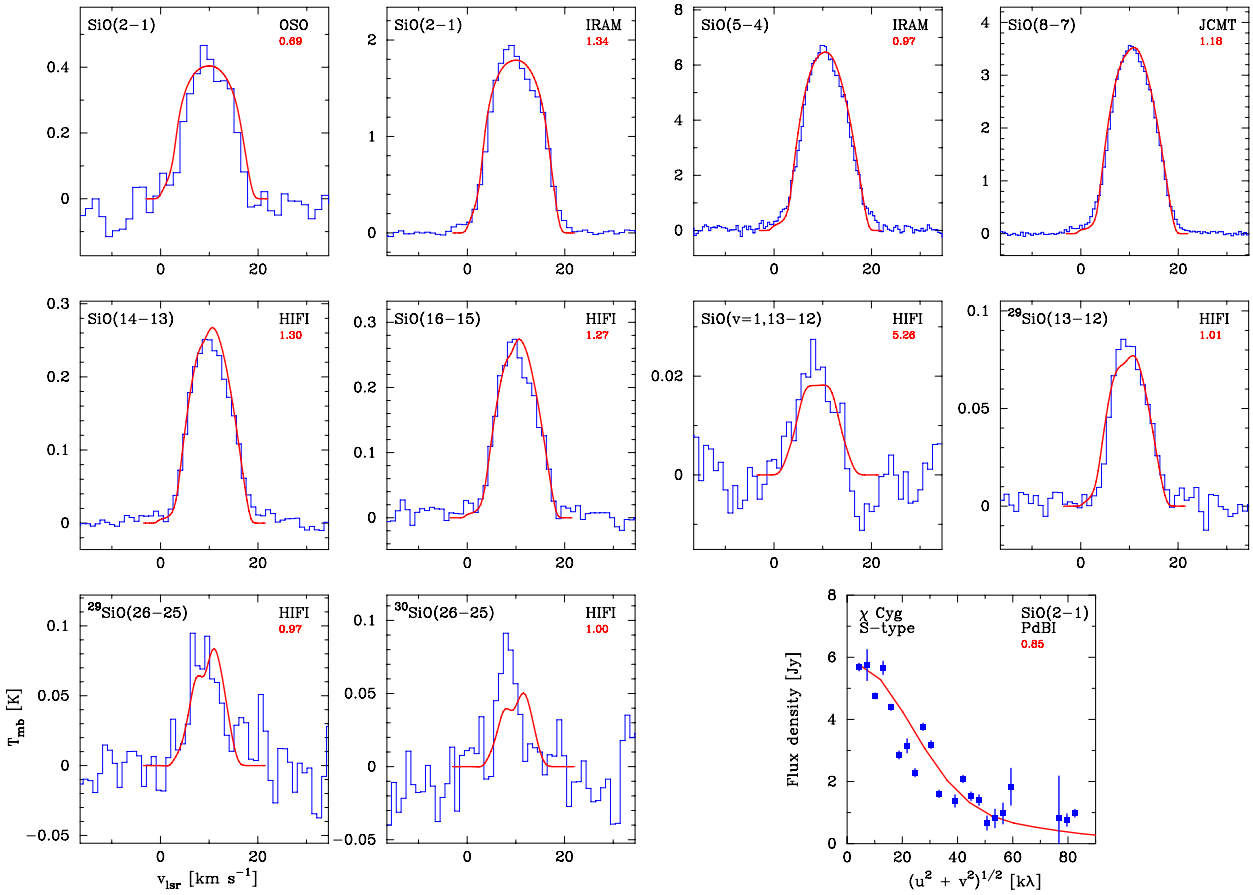

Fig. 6. SiO model (solid lines) for the S-type AGB-star χ Cyg overlaid on observations (histograms). Models have been scaled by the indicated factor (obtained from requiring that the velocity-integrated intensities are equal to the observed ones). Also shown is the derived brightness distribution in the *uv*-plane (solid lines) from the model overlaid on interferometric observations using the PdBI (blue points; data from Lucas et al. 1992).

degenerate bending mode v_2. The excitation analysis includes radiative excitation through the CH stretching mode ($v_1 = 1$; also denoted 100) at 3 μm and in the bending mode ($v_2 = 1$; also denoted 010) at 14 μm. The CN stretching mode ($v_3 = 1$; also denoted 001) at 5 μm has transitions that are about 20−1000 times weaker and is not included in the analysis. In each of the vibrational levels we include rotational levels up to $J = 25$. Hyperfine splitting of the rotational levels is included only for rotational levels in the ground state up to $J = 1$ and the resulting line overlaps are accurately treated as described in Lindqvist et al. (2000). Also, *l*-type doubling in the 14 μm transitions is included, splitting the (010) vibrational level into ($01^{1c}0$) and ($01^{1d}0$). The transition probabilities and frequencies were calculated from the molecular constants of Maki (1974). Frequencies for the hyperfine transitions are obtained from the JPL database (Pickett et al. 1998). The collisional rate coefficients between rotational levels are taken from Dumouchel et al. (2010) and were calculated for temperatures in the range from 5 to 500 K, including energy levels up to $J = 25$ for collisions with He. This set of rate coefficients was subsequently scaled by a factor 1.37 to represent collisions with H_2. The collisional rate coefficients between individual hyperfine levels were then calculated using the *proportional approximation* (e.g., Keto & Rybicki 2010)

$$\gamma_{JK,J'F'} = \frac{g(J'F')}{g(J')}\gamma_{J,J'}. \quad (7)$$

The (quasi) elastic collisions ($\Delta J = 0$) between the hyperfine energy levels were obtained from the *infinite order sudden (IOS) approximation* (e.g., Neufeld & Green 1994).

The HCN envelope size of χ Cyg is not well constrained as no interferometric observations exist of this molecule. From the ground-based single-dish data we estimate that $r_e \approx 5 \times 10^{15}$ cm. Including also the two HIFI lines the fit becomes very poor. We note that this is due to the very low $J = 13 \rightarrow 12/J = 7 \rightarrow 6$ line ratio of 0.20 which is not possible to reproduce in a model with a single Gaussian fractional abundance distribution. For comparison, in the M-type AGB star IK Tau this line ratio is observed to be 0.84 (Decin et al. 2010c), more in line with such model predictions. Leaving out the $J = 13 \rightarrow 12$ transition in the analysis we obtain a good fit ($\chi^2_{\rm red} = 1.7$; 4 observed lines) to the data using an abundance of $5.0 \pm 1.0 \times 10^{-6}$. The fit to the observations for this model is presented in Fig. 7.

However, as there is no reason not to believe the low intensity of the $J = 13 \rightarrow 12$ transition the distribution of HCN molecules in the CSE around χ Cyg must depart from that of a simple Gaussian. One possibility is that very few HCN molecules are present closer to the central star than compared with regions further out. If the HCN abundance is drastically lowered (by $\sim$ two orders of magnitudes) when $r \lesssim 1 \times 10^{15}$ cm we find that all the velocity-integrated HCN line intensities can be well modelled ($\chi^2_{\rm red} = 1.6$) using an HCN fractional abundance of $\approx 6.0 \times 10^{-6}$. Currently, there is no obvious reason for such a peculiar HCN

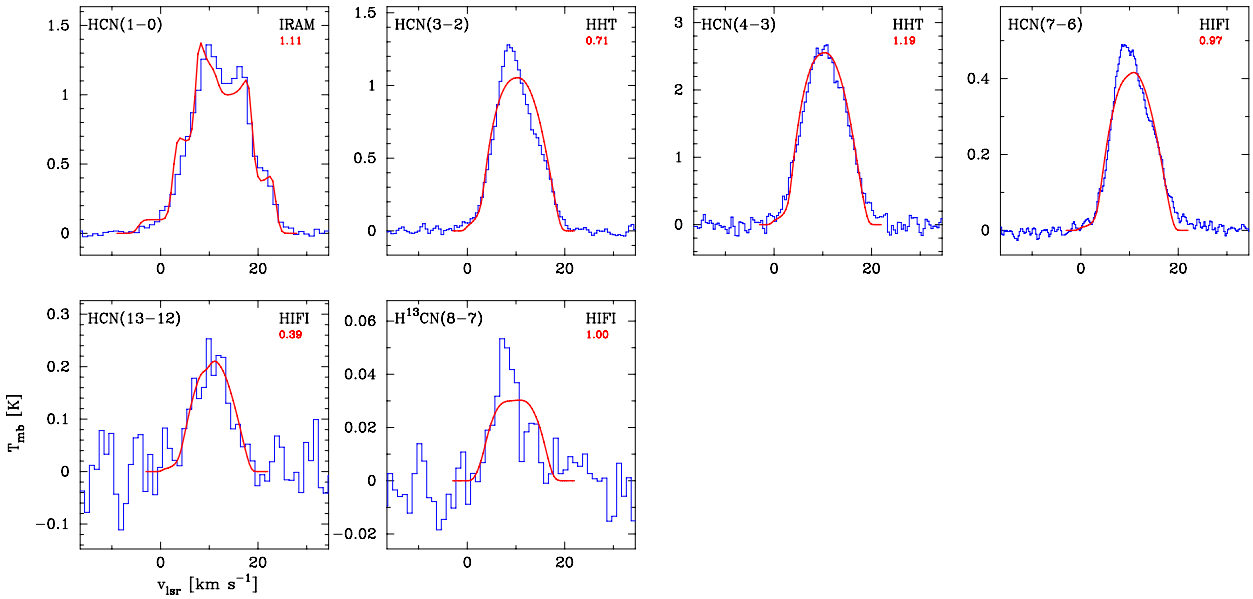

Fig. 7. HCN model (solid lines) for the S-type AGB-star χ Cyg overlaid on observations (histograms). Models have been scaled by the indicated factor (obtained from requiring that the velocity-integrated intensities are equal to the observed ones).

abundance distribution in the case of χ Cyg. Finally, we note the same tendency for an asymmetry in the line profiles as discussed above for the H_2O and SiO lines.

Weak $H^{13}CN$ line emission is also detected by HIFI for the $J = 8 \rightarrow 7$ transition. Adopting the same envelope size as for the HCN main isotope a fractional abundance of 9.0×10^{-8} (with an uncertainty of ≈50%) is obtained for $H^{13}CN$ giving an $H^{12}CN/H^{13}CN$ ratio of 56 ± 28, indicating a $^{12}C/^{13}C$ ratio consistent with that obtained from the CO modelling.

3.3.5. CN modelling

We detect strong CN line emission from two of the fine structure triplets of the $N = 6 \rightarrow 5$ rotational transition. In fact, relatively strong CN $N = 2 \rightarrow 1$ line emission was detected towards χ Cyg from the ground by Bachiller et al. (1997). They did only, however, detect very weak emission from the stronger of the two fine structure components of the CN $N = 1 \rightarrow 0$ line, suggesting relatively warm, or anomalously excited, gas. However, the size of the HCN envelope derived in Sect. 3.3.4 places the CN molecular emission in a shell at distances $>5.0 \times 10^{15}$ cm (assuming it to be the direct photodissociation product of HCN).

For CN energy levels, transition frequencies, and Einstein A-values are calculated from the spectroscopic constants of Klisch et al. (1995) together with a dipole moment of $\mu = 1.45$ Debye from Thomson & Dalby (1968). Energy levels up to $N = 11$ in both the ground ($v = 0$) and first excited vibrational state ($v = 1$), including the spin-rotation structure and the hyperfine structure, are included in the excitation analysis. The collisional rate coefficients are adopted from CO rates.

In an excitation analysis where CN is assumed to be solely produced by photodissociation of HCN (adopting a Gaussian CN distribution centered at r_e(HCN) and with a full width at the e-folding points equal to r_e(HCN) following the results of Lindqvist et al. 2000), the derived line emission cannot account for the observed CN line intensities. If the CN $N = 2 \rightarrow 1$ emision is used to constrain the model the CN $N = 1 \rightarrow 0$ emision comes out far too strong and the model CN $N = 6 \rightarrow 5$ much too weak (by about an order of magnitude). If the CN molecules instead are assumed to follow the same simple Gaussian centered on the star, as most of the other molecules, a significantly better fit ($\chi^2_{\rm red} = 2.6$ for 5 lines) is obtained adopting an envelope size of 1.0×10^{15} cm which gives an abundance of 1.9×10^{-5}. Such a small envelope size is not consistent with expectations from photodissociation alone. This may indicate that substantial amounts of CN is produced close to the star, but the derived CN line profiles for the HIFI transitions (see Fig. 8) come out too narrow, suggesting that the lines originate in a region further out in the envelope. Also, we note here that the HCN modelling suggest, on the contrary, an HCN void in the vicinity of the star.

It is clear that the CN abundance distribution around χ Cyg is more complicated than assumed here and that the limited set of observations at hand makes it very hard to put any useful constraints. High angular resolution interferometric observations may help to better constrain the CN, as well as the HCN, distribution.

3.3.6. NH_3 modelling

Here, we report an upper limit to the ortho-NH_3 $J_K = 1_0 \rightarrow 0_0$ line emission ($\int T_{\rm mb} {\rm d}v \approx 0.07\,{\rm K\,km\,s^{-1}}$) towards χ Cyg that places a significant upper limit on its fractional abundance.

For NH_3 the energy levels, transition frequencies, and Einstein A-values are taken from the HITRAN database. Energy levels up to $J = 7$ in both the ground ($v = 0$) and first excited vibrational state ($v = 1$) are included in the excitation analysis. Collisional rate coefficients are adopted from the calculations by Danby et al. (1988), for collision temperatures in the range 15 K to 300 K.

Adopting the same envelope size as for H_2O, we derive an upper limit on the total NH_3 fractional abundance of 1.8×10^{-8} (assuming an NH_3 ortho/para ratio of 1).

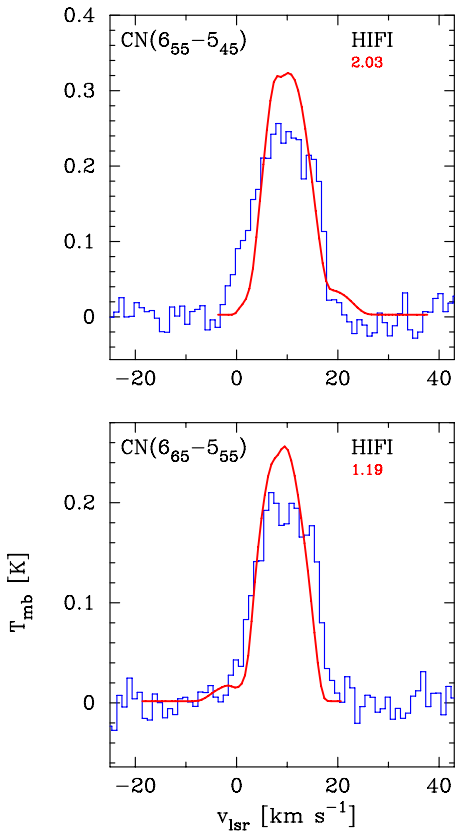

Fig. 8. CN model (solid lines) for the S-type AGB-star χ Cyg overlaid on HIFI observations (histograms). Models have been scaled by the indicated factor (obtained from requiring that the velocity-integrated intensities are equal to the observed ones). This is based on a model where the CN abundance follows a Gaussian distribution with a size r_e of 10^{15} cm.

4. Discussion

4.1. Consistency of the modelling

The dust grains and gas molecules are intricately interacting in the CSEs around AGB stars, both radiatively and dynamically. Therefore it is of interest to adopt a model that is as self-consistent as possible. Here we have adopted an approach that is self-consistent to a large degree but with some deliberate choices to break the consistency. We have two important parameters, the gas-mass-loss rate ($\dot{M}$) and the dust-to-gas mass-loss-rate ratio (Ψ) as adjustable parameters in the CO spectral line modelling as well as in the dust/dynamical modelling. In the end the constraints obtained for these two parameters from the dust and CO modelling efforts are compared and their consistency checked.

In the present modelling of χ Cyg we find that the mass-loss rates differ by 30% and the Ψ:s by 60%, i.e., they are consistent considering the uncertainties in these estimates. For instance, Ramstedt et al. (2008) report mass-loss rate uncertainties by, at least, a factor of a few for a sample of intermediate to high-mass-loss-rate objects.

4.2. Line profiles and wind dynamics

The velocity-integrated intensities, used in the χ^2 analysis for each molecular species, generally agree well with observations. This is also indicated by the reduced χ^2 values that fall in the range $\approx$1−2, see Table 3, which indicates good fits. Features such as resolved optically thin emission, increase in optical depth of lines as the rotational levels increase and self-absorption features are all remarkably well reproduced considering the simplicity of the basic assumptions of spherical symmetry and smoothness of the wind. Also the acceleration of the wind can be well reproduced by the results from a momentum-coupled wind solution. However, there is a consistent weak asymmetry in the line profiles of the H_2O, SiO and HCN lines. This can probably be attributed to small-scale deviations from spherical symmetry and the presence of a (weakly) clumped medium.

The dust/dynamical modelling performed in Sect. 3.1 gives a velocity field that can be very well approximated by Eq. (2), using $\alpha = 0.95$. This provides an excellent fit to the observed molecular lines as discussed above. However, using the molecular line spectra alone for constraining the velocity field values of α in the range $\approx$0.3−1.5 are obtained, i.e., the lines observed here only weakly constrain α. This may be due to a combination of things. The line emission normally comes from a relatively large region and hence the effect on the line shape of a velocity gradient in the acceleration region is limited. The high optical depths mean that self-absorption strongly affects the line widths. We note also that many of the, in this context particularly important, observed lines from higher energy levels have relatively low signal-to-noise ratios and are of limited use as probes of the acceleration region.

Table 3. Derived circumstellar molecular parameters.

Molecule	f_0	$r_e^\dagger$ [cm]	χ^2_{red}	N	p
CO	6.0×10^{-4}	3.5×10^{16}	1.7	10	2
^{13}CO	1.4×10^{-5}	3.5×10^{16}	0.3	3	1
ortho − H_2O	7.0×10^{-6}	3.6×10^{15}	0.8	6	1
para − H_2O	5.0×10^{-6}	3.6×10^{15}	0.6	4	1
SiO	1.3×10^{-5}	5.0×10^{16}	1.2	9	1
^{29}SiO	1.8×10^{-6}	5.0×10^{16}	0.9	2	1
^{30}SiO	7.0×10^{-7}	5.0×10^{16}	···	1	1
HCN	5.0×10^{-6}	5.0×10^{16}	1.7	5	1
H^{13}CN	8.0×10^{-8}	5.0×10^{16}	···	1	1
CN	1.9×10^{-5}	1.0×10^{15}	2.6	5	1
ortho − NH_3	$<9.0\times10^{-9}$	3.6×10^{16}	···	1	1

Notes. †Adjustable parameter fixed by other constraints (see text for details).

4.3. Molecular abundances and chemistry

It is clear that the molecular richness observed with HIFI for the S-type AGB star χ Cyg is not consistent with the results of equilibrium chemical models of stellar atmospheres, e,g,. our derived H_2O, SiO, and HCN abundances require C/O $\leq$ 0.9, $\leq$ 0.98, and $\geq$1.1, respectively, according to Cherchneff (2006). Only the SiO abundance is what can be expected from an S-star with C/O close to 1, and the H_2O and HCN abundances are inconsistent with each other. The derived circumstellar fractional abundances relative to H_2 are shown in Fig. 9, and summarized in Table 3, which present a chemistry (over the HIFI bands), comparable to that observed for the high mass loss rate M-type AGB star IK Tau, recently published in Decin et al. (2010b,c). Shock-induced chemistry (Cherchneff 2006) or clumpiness (Agúndez et al. 2010) may provide an explanation to the observed abundances.

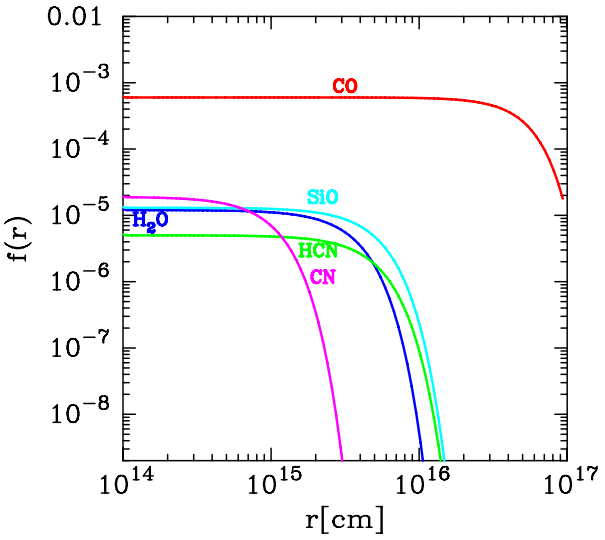

Fig. 9. The chemistry in the CSE of χ Cyg.

4.4. Oxygen-bearing molecules

For H_2O we derive an ortho-H_2O abundance of 7.0×10^{-6} and a para-H_2O abundance of 5.0×10^{-6}. The total H_2O abundance is then $\approx1.2\times10^{-5}$ placing it in between the values typically determined for M-type AGB stars (Justtanont et al. 2005; Maercker et al. 2008, 2009; Decin et al. 2010c) and carbon stars (Melnick et al. 2001; Hasegawa et al. 2006; Decin et al. 2010a; Neufeld et al. 2010, 2011). Justtanont et al. (2010) derived a total H_2O abundance of $\approx1.1\times10^{-5}$ for χ Cyg in excellent agreement with the analysis performed here. The derived circumstellar o/p-ratio of 1.4 ± 0.34 (corresponding to a temperature of about 50 K), is significantly less than the high-temperature equilibrium value of 3, indicating formation of H_2O in non-LTE conditions. We note that Justtanont et al. (2010) obtained a circumstellar o/p-ratio of 2.1 ± 0.6 (based on fewer H_2O emission lines), consistent within the mutual uncertainties.

Also, we find that line cooling from H_2O is only important in a small region of the CSE very close to the central star ($\lesssim6.0\times10^{14}$ cm).

The circumstellar SiO fractional abundance obtained is 1.3×10^{-5}, more than an order of magnitude higher than obtained in thermal equilibrium chemistries, but in line with non-equilibrium models (Cherchneff 2006). We also note that rotational lines from the first vibrationally excited state come out too weak in this model. One possible explanation for this is that the abundance of SiO is higher in the warmer region closer to the star (Schöier et al. 2004; Schöier et al. 2006a,b; Decin et al. 2010b). This could be an effect due to adsorption of SiO onto dust grains in the dust forming region, that lowers the SiO fractional abundance farther out in the wind.

4.5. Carbon-bearing molecules

The excitation analysis of the HCN and CN line emission detected by HIFI does not come out as expected. Model line emission from the HCN $J=13\rightarrow12$ transition comes out far too strong and requires the HCN fractional abundance to be lowered in regions $\lesssim1.0\times10^{15}$ cm. For CN, on the other hand, the abundance distribution appears to be peaked on the central star, in conflict with models that predict it to be mainly the photodissociation product of circumstellar HCN and thus should appear in a shell-like structure around the star. It is very difficult to explain such a scenario based on current chemical models. Possibly, a shock-induced chemistry which is very sensitive to the physical conditions could be important, as the C/O ratio appears to only have a minor effect for S-stars (Cherchneff 2006). Also clumpiness can possibly lead to chemical signatures that deviate from the expected (Agúndez et al. 2010; Decin et al. 2010a).

4.6. Isotope ratios

From the CO analysis we derive a $^{12}CO/^{13}CO$-ratio of 43 ± 6 and from HCN an $H^{12}CN/H^{13}CN$ ratio of 56 ± 28. This suggests a $^{12}C/^{13}C$ isotopic ratio that is higher than what is found in M-type AGB stars (Knapp & Chang 1985; Milam et al. 2009) and more in line with those derived for carbon stars (Knapp & Chang 1985; Schöier & Olofsson 2000; Milam et al. 2009). However, we note here that Hinkle et al. (1976) derive a $^{12}CO/^{13}CO$-ratio of 25 ± 7 from CO vibrational lines (i.e., from lines originating in the stellar atmosphere) and that Milam et al. (2009) derive a ratio of 33 from CO radio lines.

The SiO analysis gives a $^{28}SiO/^{29}SiO$ abundance ratio of 8 ± 2 and a $^{28}SiO/^{30}SiO$ abundance ratio of 19 ± 8. These isotopic ratios can be compared with the $^{28}Si/^{29}Si$ and $^{28}Si/^{30}Si$ ratios inferred for the Sun (19 and 29, respectively), IK Tau (27 and 80, respectively, Decin et al. 2010c), and IRC+10216 (15 and 20, respectively). Thus, the χ Cyg results are more in line with those of the Sun and the carbon star IRC+10216 than those of the M-type star IK Tau, but we warn that our results are based on only two ^{29}SiO lines and one ^{30}SiO line.

4.7. NH_3

Recently, Menten et al. (2010) presented HIFI observations of the ortho-NH_3 $J_K=1_0\rightarrow0_0$ transition for a sample of four oxygen-rich evolved stars. They report relatively high NH_3 abundances in the range from 2×10^{-7} to 3×10^{-6}. NH_3 $J_K=1_0\rightarrow0_0$ line emission has also been detected towards the carbon star IRC+10216 using the Odin satellite (Hasegawa et al. 2006). The derived ortho-NH_3 abundance is 1×10^{-6}. However, these works did not include the possibility of IR pumping via vibrationally excited states in the radiative transfer analysis. We find that including the $v=1$ vibrational state lowers the derived fractional abundance in χ Cyg by approximately an order of magnitude. This suggests that the NH_3 abundances quoted in Hasegawa et al. (2006) and Menten et al. (2010) should generally be lowered by about an order of magnitude. The upper limit of 1.8×10^{-8} derived for χ Cyg possibly indicates that circumstellar NH_3 abundance is lower in S-stars than in other AGB stars, however the statistics are very poor.

5. Conclusions

Here we summarize the main conclusions reached in the paper.

- The observed HIFI spectrum, in the range from ≈550 GHz to 1.9 THz, of the S-type AGB star χ Cyg is relatively rich in spectral lines from common molecules such as CO, H_2O and SiO (and some of their isotopologues). Carbon bearing molecules such as HCN and CN are detected at lower abundances.
- Based on the detailed dust continuum radiative transfer and molecular line radiative transfer that has been performed, we find no evidence that the mass loss rate from χ Cyg has varied significantly in time during the past ≈1000 yr. The constraints on the acceleration region in the stellar wind is

Table A.1. References for complementary spectral line data.

Reference	Telescope	Transition	$\int T_{\rm mb} {\rm d}\upsilon$ [K km s^{-1}]
Ramstedt et al. (2009)	OSO	CO(1–0)	27.2
	IRAM	CO(1–0)	70.9
	JCMT	CO(2–1)	60.2
	IRAM	CO(2–1)	265.8
	JCMT	CO(3–2)	119.5
	JCMT	CO(4–3)	134.6
Schöier et al. (in prep.)	APEX	CO(3–2)	88.6
Ramstedt et al. (2009)	OSO	SiO(2–1)	4.5
	IRAM	SiO(2–1)	23.1
	IRAM	SiO(5–4)	72.3
	JCMT	SiO(8–7)	38.1
Schöier et al. (in prep.)	IRAM	HCN(1–0)	19.2
Bieging et al. (2000)	HHT	HCN(3–2)	12.3
	HHT	HCN(4–3)	29.0

consistent between the dust modelling and the molecular line analysis.

- For H_2O we derive an ortho-H_2O abundance of 7.0×10^{-6} and a para-H_2O abundance of 5.0×10^{-6}. The total H_2O abundance is then $\approx1.2\times10^{-5}$ placing it inbetween the values typically determined for M-type AGB stars and carbon stars. The derived o/p-ratio of 1.4 ± 0.34, is significantly less than the high-temperature equilibrium value of 3, indicating formation of H_2O in non-LTE conditions. Also, we find that line cooling from H_2O is only important in a small region of the CSE very close to the central star ($\lesssim6.0\times10^{14}$ cm).
- The detection of carbon bearing molecules such as HCN and CN requires non-LTE chemical processes to explain their, in this context, high abundances. However, we fail to fit consistently the combined ground-based and HIFI data for HCN and CN. Possibly, their spatial distributions in the CSE are different than assumed based on current chemical models.
- Many of the H_2O, SiO, and HCN lines show an asymmetry in the line profile in the sense that the line shape peak is shifted slightly to the blue.
- From the CO analysis we derive a ^{12}CO/^{13}CO ratio of 43 ± 6 and from HCN an H^{12}CN/H^{13}CN ratio of 56 ± 28. These values suggest a ^{12}C/^{13}C isotopic ratio that is higher than what is found in M-type AGB stars (Knapp & Chang 1985; Milam et al. 2009) and more in line with those derived for carbon stars (Knapp & Chang 1985; Schöier & Olofsson 2000; Milam et al. 2009).

Acknowledgements. F.L.S., M.M., K.J., and H.O. acknowledge financial support from the Swedish National Space Board and the Swedish Research Council.

Appendix A: Ground based molecular line observations used in the analysis

Listed in Table A.1 are the references to the ground-based molecular line observations used in combination with the HIFI data in the molecular excitation analysis performed in Sect. 3. The total velocity-integrated intensity ($\int T_{\rm mb} {\rm d}\upsilon$) is also listed for each transition.

Appendix B: Continuum observations used in the analysis

Listed in Table B.1 are the continuum observations used to form the SED of χ Cyg shown in Fig. 2. In addition, SWS and LWS spectra from the ISO satellite (obtained from the ISO data archive[1]) are shown in the SED, however these are not used in the χ^2-analysis in Sect. 3.

Table B.1. References for continuum data.

Reference	Telescope	λ [μm]	F_ν [Jy]
Skrutskie et al. (2006)	2MASS	1.24	1362.0
	2MASS	1.64	2812.0
	2MASS	2.16	3178.0
Beichman et al. (1988)	IRAS	12.0	1688.0
	IRAS	25.0	459.0
	IRAS	60.0	80.67
	IRAS	100.0	17.72
Castro – Carrizo et al. (2010)	IRAM PdBI	1300.0	0.065
	IRAM PdBI	2300.0	0.0158

References

Agúndez, M., Cernicharo, J., & Guélin, M. 2010, ApJ, 724, L133
Bachiller, R., Fuente, A., Bujarrabal, V., et al. 1997, A&A, 319, 235
Beichman, C., Neugebauer, G., Habing, H., et al. 1988, Infrared Astronomical Satellite (IRAS) Catalogs and Atlases, vol. 1, Explanatory Supplement, NASA RP-1190 (Washington, DC: GPO)
Bieging, J. H., Shaked, S., & Gensheimer, P. D. 2000, ApJ, 543, 897
Castro-Carrizo, A., Quintana-Lacaci, G., Neri, R., et al. 2010, A&A, 523, A59
Chandra, S., Maheshwari, V. U., & Sharma, A. K. 1996, A&AS, 117, 557
Cherchneff, I. 2006, A&A, 456, 1001
Crosas, M., & Menten, K. M. 1997, ApJ, 483, 913
Danby, G., Flower, D. R., Valiron, P., Schilke, P., & Walmsley, C. M. 1988, MNRAS, 235, 229
Dayou, F., & Balança, C. 2006, A&A, 459, 297
Decin, L., Agúndez, M., Barlow, M. J., et al. 2010a, Nature, 467, 64
Decin, L., de Beck, E., Brünken, S., et al. 2010b, A&A, 516, A69
Decin, L., Justtanont, K., de Beck, E., et al. 2010c, A&A, 521, L4
Dumouchel, F., Faure, A., & Lique, F. 2010, MNRAS, 406, 2488
Faure, A., Crimier, N., Ceccarelli, C., et al. 2007, A&A, 472, 1029
Goldreich, P., & Scoville, N. 1976, ApJ, 205, 144
Hasegawa, T., Kwok, S., Koning, N., et al. 2006, ApJ, 637, 791
Hinkle, K. H., Lambert, D. L., & Snell, R. L. 1976, ApJ, 210, 684
Huggins, P. J., Mauron, N., & Wirth, E. A. 2009, MNRAS, 396, 1805
Ivezićs, Ž., & Elitzur, M. 1997, MNRAS, 287, 799
Justtanont, K., & Tielens, A. G. G. M. 1992, ApJ, 389, 400
Justtanont, K., Bergman, P., Larsson, B., et al. 2005, A&A, 439, 627
Justtanont, K., Decin, L., Schöier, F. L., et al. 2010, A&A, 521, L6
Keady, J. J., & Ridgway, S. T. 1993, ApJ, 406, 199
Keto, E., & Rybicki, G. 2010, ApJ, 716, 1315
Kholopov, P. N., Samus, N. N., Frolov, M. S., et al. 1999, VizieR Online Data Catalog, 2214, 0
Klisch, E., Klaus, T., Belov, S. P., Winnewisser, G., & Herbst, E. 1995, A&A, 304, L5
Knapp, G. R., & Chang, K. M. 1985, ApJ, 293, 281
Knapp, G. R., Pourbaix, D., Platais, I., & Jorissen, A. 2003, A&A, 403, 993
Lamers, H. J. G. L. M., & Cassinelli, J. P. 1999, Introduction to Stellar Winds, ed. H. J. G. L. M. Lamers, & J. P. Cassinelli
Lindqvist, M., Schöier, F. L., Lucas, R., & Olofsson, H. 2000, A&A, 361, 1036
Lucas, R., Bujarrabal, V., Guilloteau, S., et al. 1992, A&A, 262, 491
Müller, H. S. P., Thorwirth, S., Roth, D. A., & Winnewisser, G. 2001, A&A, 370, L49
Müller, H. S. P., Schlöder, F., Stutzki, J., & Winnewisser, G. 2005, J. Mol. Struct., 742, 215
Maercker, M., Schöier, F. L., Olofsson, H., Bergman, P., & Ramstedt, S. 2008, A&A, 479, 779
Maercker, M., Schöier, F. L., Olofsson, H., et al. 2009, A&A, 494, 243
Maki, A. G. 1974, J. Phys. Chem. Ref. Data, 3, 221
Mauron, N., & Huggins, P. J. 1999, A&A, 349, 203
Mauron, N., & Huggins, P. J. 2000, A&A, 359, 707

[1] Based on observations with ISO, an ESA project with instruments funded by ESA Member States (especially the PI countries: France, Germany, the Netherlands and the United Kingdom) and with the participation of ISAS and NASA.

Mauron, N., & Huggins, P. J. 2006, A&A, 452, 257
Melnick, G. J., Neufeld, D. A., Ford, K. E. S., Hollenbach, D. J., & Ashby, M. L. N. 2001, Nature, 412, 160
Menten, K. M., Wyrowski, F., Alcolea, J., et al. 2010, A&A, 521, L7
Milam, S. N., Woolf, N. J., & Ziurys, L. M. 2009, ApJ, 690, 837
Netzer, N., & Knapp, G. R. 1987, ApJ, 323, 734
Neufeld, D. A., & Green, S. 1994, ApJ, 432, 158
Neufeld, D. A., González-Alfonso, E., Melnick, G., et al. 2010, A&A, 521, L5
Neufeld, D. A., González-Alfonso, E., Melnick, G., et al. 2011, ApJ, 727, L29
Ng, K. 1974, J. Chem. Phys., 61, 2680
Pickett, H. M., Poynter, R. L., Cohen, E. A., et al. 1998, J. Quant. Spect. Radiat. Transf., 60, 883
Raymonda, J. W., Muenter, J. S., & Klemperer, W. A. 1970, J. Chem. Phys., 52, 3458
Ramstedt, S., Schöier, F. L., Olofsson, H., & Lundgren, A. A. 2006, A&A, 454, L103
Ramstedt, S., Schöier, F. L., Olofsson, H., & Lundgren, A. A. 2008, A&A, 487, 645
Ramstedt, S., Schöier, F. L., & Olofsson, H. 2009, A&A, 499, 515
Rybicki, G. B., & Hummer, D. G. 1991, A&A, 245, 171
Rybicki, G. B., & Hummer, D. G. 1992, A&A, 262, 209
Ryde, N., Schöier, F. L., & Olofsson, H. 1999, A&A, 345, 841
Schöier, F. L., & Olofsson, H. 2000, A&A, 359, 586
Schöier, F. L., & Olofsson, H. 2001, A&A, 368, 969
Schöier, F. L., Ryde, N., & Olofsson, H. 2002, A&A, 391, 577
Schöier, F. L., Olofsson, H., Wong, T., Lindqvist, M., & Kerschbaum, F. 2004, A&A, 422, 651
Schöier, F. L., van der Tak, F. F. S., van Dishoeck, E. F., & Black, J. H. 2005, A&A, 432, 369
Schöier, F. L., Fong, D., Olofsson, H., Zhang, Q., & Patel, N. 2006a, ApJ, 649, 965
Schöier, F. L., Olofsson, H., & Lundgren, A. A. 2006b, A&A, 454, 247
Skrutskie, M. F., Cutri, R. M., Stiening, R., et al. 2006, AJ, 131, 1163
Thomson, R., & Dalby, F. W. 1968, Can. J. Phys., 46, 2815
van der Tak, F. F. S., Black, J. H., Schöier, F. L., Jansen, D. J., & van Dishoeck, E. F. 2007, A&A, 468, 627
van Zadelhoff, G., Dullemond, C. P., van der Tak, F. F. S., et al. 2002, A&A, 395, 373
Willacy, K. 2004, ApJ, 600, L87
Yang, B., Stancil, P. C., Balakrishnan, N., & Forrey, R. C. 2010, ApJ, 718, 1062